Cascaded coherent anti-Stokes Raman scattering for high-sensitivity number density determination in the gas phase

Kliukin, Dmitrii; Mazza, Francesco; Castellanos, Leonardo; Bohlin, Alexis

DOI
10.1002/jrs.6120

Publication date
2021

Document Version
Final published version

Published in
Journal of Raman Spectroscopy

Received: 30 December 2020 | Revised: 4 March 2021 | Accepted: 5 April 2021

DOI: 10.1002/jrs.6120

SPECIAL ISSUE - RESEARCH ARTICLE

Journal of RAMAN SPECTROSCOPY WILEY

Cascaded coherent anti-Stokes Raman scattering for high-sensitivity number density determination in the gas phase

Dmitrii Kliukin | **Francesco Mazza** | **Leonardo Castellanos** | **Alexis Bohlin**

Faculty of Aerospace Engineering, Delft University of Technology, Delft, The Netherlands

Correspondence
Alexis Bohlin, Faculty of Aerospace Engineering, Delft University of Technology, Kluyverweg 1, 2629 HS Delft, The Netherlands.
Email: g.a.bohlin@tudelft.nl

Funding information
Netherlands Organization for Scientific Research, Grant/Award Number: 15690

Abstract

Cascaded coherent anti-Stokes Raman scattering (CARS) signals can be efficiently generated from CARS signals when propagating collinearly with the pump/Stokes and probe beams. This effect can be seen as the CARS beam acting as the probe beam and being inelastically scattered a 'second time' from the Raman coherence induced along the focus of the pump/Stokes beam axis. Although much weaker, this additionally scattered signal co-propagates with the CARS signal and may complicate the analysis of the CARS spectrum used for diagnostics in the gas phase. In particular, the occurrence of the cascaded CARS process needs to be taken into account analysing minor spectral signatures at relatively high number density of scattering molecules. Here we show how polarization control can be employed to generate CARS and cascaded CARS signals with orthogonal linear polarization and how, in this way, the cascaded CARS signals can be efficiently suppressed. However, instead of rejecting this signal, we collect both the generated CARS and cascaded CARS signals on the same detector frame, and we explore the use of these counterparts for absolute concentration measurements of the Raman-active species. The cascaded CARS signal has exponential-order higher sensitivity to the number density of the scattering molecules in the mixture. We demonstrate that the ratio of the CARS and the cascaded CARS signals is independent of the probe pulse energy in use, which can be a promising approach for wide-range absolute concentration measurements in gas-phase media.

KEYWORDS

gas-phase thermometry, in-situ pressure monitoring, laser diagnostics, nonlinear optical spectroscopy, polarization control

1 | INTRODUCTION

Coherent anti-Stokes Raman scattering (CARS) spectroscopy is a powerful laser diagnostic technique for nonintrusive, high-fidelity thermometry in chemically reacting flows.[1] Time-resolved CARS spectroscopy, branching to its chirped-probe pulse (CPP)[2,3] and hybrid femtosecond/picosecond (fs/ps)[4] implementations, has demonstrated unprecedented values of precision (~1%) and accuracy (<3%) for flame thermometry.[5,6] Moreover, the possibility of suppressing the nonresonant four-wave mixing signal

due to the electronic susceptibility of the medium, and the near-independence of the CARS spectrum of molecular collisions up to 70 bar, make hybrid fs/ps CARS a viable diagnostic technique in high-pressure environments.[7] In addition to quantifying temperature, pure-rotational fs/ps CARS can readily provide relative concentrations of O_2, N_2 and H_2,[8,9] as well as the measurement of pressure and dephasing coefficients performed in dual-probe or multiprobe arrangements,[10–12] respectively. In the CARS process, the Raman coherence is induced by the two-photon interaction of the Raman-active molecule with a pump and a Stokes photon. Subsequently, a third photon, termed the 'probe' photon, is inelastically scattered by the molecule, producing a fourth photon at a higher wavenumber: the CARS photon.[1] It has been reported in the literature[13] that, under specific conditions, the CARS process can be accompanied by an additional optical process, referred to as 'cascaded CARS' (CCARS). Under such conditions, the amplitude of the CARS field is large enough to significantly couple to the molecular susceptibility of the optical medium, resulting in a CCARS field generated with an additional Raman shift. There are two forms of CCARS processes, termed 'sequential' and 'parallel', which are produced through different pathways.[13] In the parallel process, the CARS photon serves as a probe photon in a secondary scattering process, whereas in the sequential one the CARS photon participates in the creation of the Raman coherence. It has been demonstrated that the parallel CCARS pathway is more probable than the sequential one.[14] The generation of CCARS signals in gas-phase media has been observed in various settings, an example being the hollow-core fibres—filled with CO_2, N_2, H_2—used for ultra-broadband light generation in the spectral range from vacuum-UV to mid-infrared (IR).[15–17] The increase in spectral bandwidth of the propagating pulse was observed due to self-phase modulation, stimulated Raman scattering and CCARS. Recently, the generation of a CCARS signal up the 58^{th} order in gaseous CO_2 has been reported.[18] This was achieved with a collinearly focused femtosecond pump/Stokes and a picosecond probe pulse produced by N_2^+ lasing. The resulting CCARS signal had enough bandwidth to excite the Q-branch Raman transitions in the CO_2 Fermi dyad at $\sim$1300 cm^{-1}. A similar result has been achieved by single-beam CARS, starting directly from an ultra-broadband source to provide the pump/Stokes pulse.[19] A CCARS signal was also observed, in the context of CARS microscopy, from biomolecules in a cell, and compared to higher order $\chi^{(5)}$ nonlinear optical processes.[20,21] The benefit of using the CCARS signal in imaging microscopy is that a higher spectral resolution can be achieved than with a direct $\chi^{(3)}$ process.

In the present work, we investigate the use of CCARS for high-sensitivity determination of the number density of Raman-active species in the gas phase. This is performed through a quantitative analysis of the CCARS and CARS signals simultaneously generated in a binary mixture of nitrogen and argon, at ambient temperature and pressure. We validate a phenomenological description of the dependence of the CCARS signal on the number density of molecular scatterers and on the intensity of the pump/Stokes and probe pulses. We generate the CARS and the CCARS signals with orthogonal polarization, in order to separate and simultaneously detect them within a single detector frame. The CARS signal is employed for thermometry, while the ratio of CARS and CCARS is employed to determine the number density of nitrogen in the mixture with argon.

2 | BASICS

2.1 | Time-domain CARS model

In the present work, we make use of the time-domain CARS model detailed in Miller et al.,[22] and we further develop it to describe the CCARS process. The pump, Stokes and probe pulses are assumed to be transform limited, although the model can be extended to include chirp in the spectrum of the probe laser pulse.[23] The energy diagram of a molecule undergoing a pure-rotational Raman transition within a single vibrational band is depicted in Figure 1a. The pump and Stokes constructive photon pairs, found across the entire broad bandwidth of a single femtosecond pulse, coherently excite the Raman-active molecules between rotational energy states, according to the selection rule: $J \rightarrow J+2$. After a time delay τ, the probe photons are inelastically scattered from these molecules resulting in the CARS polarization field. The third-order polarization, $P^{(3)}_{CARS}$, thus induced in the gas-phase medium can be described, in the time domain, as the convolution of the three input laser fields with the nonlinear molecular response:

$$P^{(3)}_{CARS}(t,\tau) = \left(\frac{i}{h}\right)^3 E_3(t) e^{i\omega_3 t} \int_0^\infty \chi^{(3)}(t_2) E_2^*(t+\tau-t_2) E_1(t+\tau-t_2) e^{i(\omega_1-\omega_2)t_2} dt_2, \quad (1)$$

where E_1, E_2 and E_3 are the pump, Stokes and probe pulse electric field envelopes, ω_1, ω_2 and ω_3 are the corresponding angular frequencies, and τ is the time delay between the combined pump/Stokes pulse and the probe pulse. The molecular response function $\chi^{(3)}(t)$

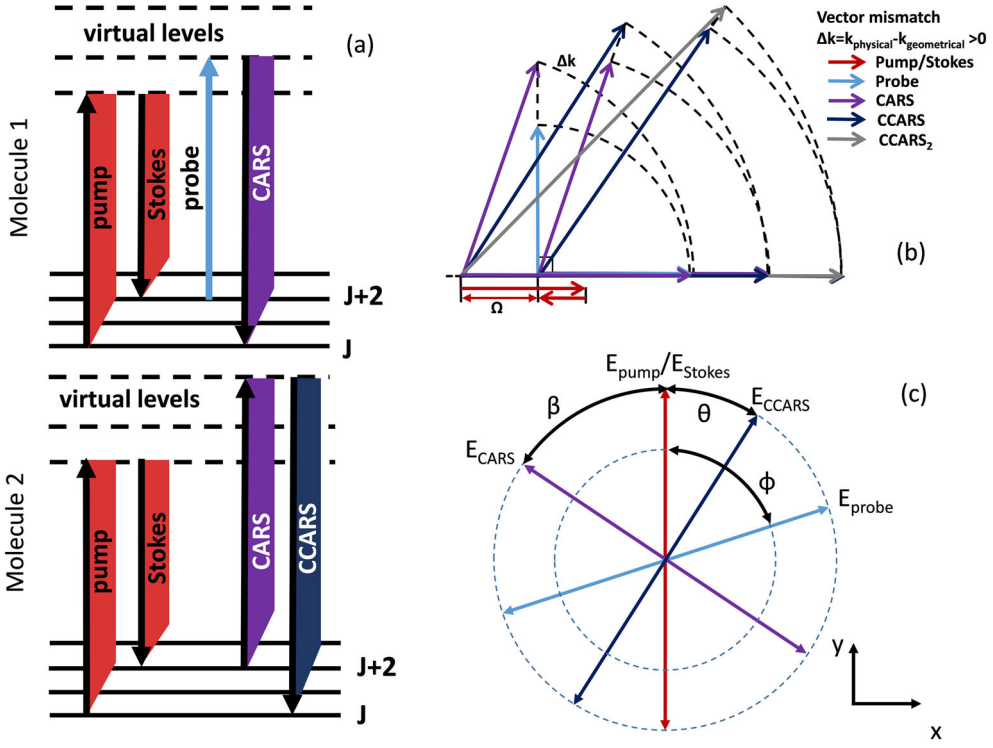

FIGURE 1 (a) Energy diagram of coherent anti-Stokes Raman scattering (CARS) and cascaded CARS (CCARS). (b) The two-beam phase-matching diagram for CARS, with all-collinear beams and the probe pulse orthogonal to the pump/Stokes pulse. The cascaded CARS signal is generated by the CARS field acting as a probe beam. (c) The polarization settings to generate the CARS and CCARS fields with orthogonal polarization states ($\beta + \theta = 90°$) [Colour figure can be viewed at wileyonlinelibrary.com]

includes all the rotational transitions from the initial states (J) to the final states ($J + 2$), according to the selection rule of the pure-rotational CARS process:

$$\chi^{(3)}(t) = \sum\nolimits_J a_{J,J+2} e^{-i\omega_{J,J+2}t - \Gamma_{J,J+2}t}. \quad (2)$$

Here, $\Gamma_{J,J+2}$ is a transition linewidth corresponding to the state-dependent dephasing of the rotational coherence, and $\omega_{J,J+2}$ is the transition angular frequency. The transition strength is expressed as $a_{J,J+2} \propto \frac{4}{45}\frac{N}{\hbar}\xi^2 b_{J,J+2} F_J \Delta\rho_{J,J+2}$, with $\Delta\rho_{J,J+2}$ being the Boltzmann population difference factor between the initial and final rotational states, $b_{J,J+2}$ the Placzek–Teller coefficient, F_J the Herman–Wallis factor, ξ the polarizability anisotropy and N the number density of the scattering species. The model is presently limited to the ground vibrational state, which is the only one significantly populated at room temperature, but it can be easily extended to include higher vibrational states, at higher temperatures. The final expression for the CARS signal intensity is[24] as follows:

$$I^{(3)}_{CARS} = \left|P^{(3)}_{CARS}\right|^2 \propto \left|\chi^{(3)}\right|^2 \left(\frac{\omega_{CARS}}{c}\right)^2 I_1 I_2 I_3 \Delta z^2, \quad (3)$$

Here, I_1, I_2 and I_3 are the intensities of the pump, Stokes and probe pulses, Δz is the interaction length, ω_{CARS} is the carrier frequency of the CARS signal, and c is the speed of light. The expression does not include the phase-matching term as in this study we only employ a collinear scheme, for which all beams are propagating along the same axis and the phase-matching condition is automatically satisfied.[24] The effect of the phase-mismatch should be taken into account for large crossing angles in the two-beam CARS scheme.[25] However, it is interesting that for the CCARS signal the phase-mismatch is decreased for every increased scattering order, as displayed in Figure 1b. A detailed analysis of this effect is beyond the scope of the present study, but it might be important for ultra-broadband CARS applications, where the Raman coherence is also induced at significantly larger Raman shifts.[26]

2.2 | Cascaded CARS

As the CARS photons propagate through the medium, they interact with the Raman-active molecules resulting in a second coherent Raman scattering process. This is the origin of the CCARS photons, as shown in Figure 1a. Since the spectrum of the CARS signal is discrete in nature, with spectral lines corresponding to the rotational transition wavenumbers, each of its spectral components gives rise to its own rotational CCARS spectrum. Therefore, the time-domain CCARS polarization can be modelled by Equation 3 by substituting P_{CARS} as the probe field:

$$P^{(3)}_{CCARS}(t,\tau)=\left(-\frac{i}{\hbar}\right)^3 P^{(3)}_{CARS}(t,\tau)\int_0^\infty \chi^{(3)}(t_2)E_2^*(t+\tau-t_2)E_1(t+\tau-t_2)e^{i(\omega_1-\omega_2)t_2}dt_2. \tag{4}$$

Following the derivation in Gong et al.,[21] the intensity of the CCARS signal can be calculated as follows:

$$I^{(3)}_{CCARS}=\left|P^{(3)}_{CCARS}\right|^2 \propto \left|\chi^{(3)}\right|^2\left(\frac{\omega_{CCARS}}{c}\right)^2 I_1 I_2 I_{CARS}\Delta z^2 \propto \left|\chi^{(3)}\right|^4\left(\frac{\omega_{CARS}\omega_{CCARS}}{c^2}\right)^2 I_1^2 I_2^2 I_3 \Delta z^4. \tag{5}$$

The CCARS signal has a quadratic dependence on the intensity of both the pump and the Stokes pulses, similarly to a direct $\chi^{(5)}$ process.[21] The linewidth employed in the modelling of the CARS signal can be also applied to the CCARS signal, because both are generated from the same probe volume described with common $\chi^{(3)}$. In this work, the phase-matching condition is fulfilled for CCARS with a collinear two-beam scheme providing long enough an interaction length, $\Delta z = 3$ mm. With BOX-CARS geometry, the interaction length would be considerably shorter (~1 mm) reducing the generation efficiency of CCARS signal. It is also clear that the CCARS signal has a stronger dependence on the number density of the scattering species $I^{(3)}_{CCARS}\sim N^4$, in comparison to the CARS signal, for which the dependence is known to be $I^{(3)}_{CARS}\sim N^2$. In addition, the ratio of the CARS and the CCARS signals does not depend on the probe pulse intensity and can be expressed as follows:

$$\frac{I^{(3)}_{CCARS}}{I^{(3)}_{CARS}}\propto\left|\chi^{(3)}\right|^2\left(\frac{\omega_{CCARS}}{c}\right)^2 I_1 I_2 \Delta z^2. \tag{6}$$

2.3 | Polarization separation of CARS and CCARS

The orientation of a linearly polarized CARS signal is determined by the third-order susceptibility tensor of the gas-phase medium and by the relative incident linear polarization of the pump, Stokes and probe pulses. Polarization suppression of the nonresonant CARS signal,[27] or of the near collinearly propagating probe beam in two-beam CARS setups,[25] has been routinely employed in CARS spectroscopy. In the case of two-beam CARS, a single fs pulse provides the pump and Stokes photons, which thus have the same polarization state. In Figure 1c, the polarization settings for two-beam CARS are presented, following the notation in Vestin et al.[28]

The CARS polarization angle β, relative to the polarization of the pump/Stokes beam, can be calculated as follows:

$$\tan\beta=-\frac{1}{2}\tan\phi, \tag{7}$$

where ϕ is the relative polarization angle between the pump/Stokes and the probe beams. In the CCARS signal generation process, the CARS signal acts as the probe; therefore, the polarization angle of the CCARS signal (θ), relative to the pump/Stokes beam, can be calculated as follows:

$$\tan\theta=-\frac{1}{2}\tan\beta=\frac{1}{4}\tan\phi. \tag{8}$$

One can thus generate the CARS and CCARS signals with orthogonal relative polarization when the angle ϕ is set to 70.5°.

3 | EXPERIMENTAL DETAILS

The experiment is carried out with a two-beam fs/ps CARS setup equipped with polarization-sensitive divided detection, as described in detail in Mazza et al.[29] A schematic of such a setup is provided in Figure 2. The pump/Stokes and probe pulses are generated from a single ultrafast regenerative amplifier system (Astrella, Coherent) with two separate output beams, at 800-nm wavelength. The first output serves as the combined pump/Stokes beam with an ~35-fs pulse duration. The second output beam is fed to a second harmonic bandwidth compressor (SHBC, Light conversion), employed to generate an ~5-ps duration probe pulse at 400-nm wavelength. The path-length difference between the synchronized pump/Stokes and probe pulses arriving to the experiment is compensated for by an optical delay line, and the relative arrival time is controlled by an automated translation stage (Thorlabs, sub-10-fs resolution). A spatial 4f-filter in transmission is mounted in the probe beam path to tune the probe bandwidth, resulting in an ~15-ps pulse duration for this experiment, and a corresponding maximum pulse energy of ~500 μJ. The measurements are performed at ~30-ps probe delay with efficient temporal gating of the nonresonant CARS signal. The pulse energy of both beams is attenuated for the current experiment, operating at a maximum of ~120 μJ/pulse for the pump/Stokes pulse and at ~16 μJ/pulse for the probe pulse. Both the pump/Stokes and probe beams are focused to the measurement location in the gaseous flow with spherical lenses ($f_{p/St}$ = 500 mm, f_{pr} = 300 mm)

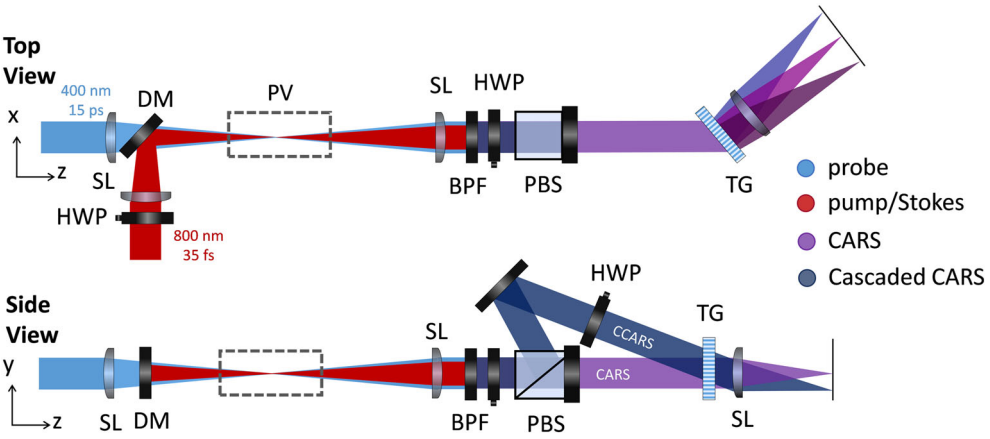

FIGURE 2 Polarization-divided detection of the coherent anti-Stokes Raman scattering (CARS) and cascaded CARS signals. BPF, band-pass filter; DM, dichroic mirror; HWP, half-wave plate; PBS, polarization beam splitter; PF, measurement location placed within a pipe flow; SL, spherical lens; TG, transmission grating [Colour figure can be viewed at wileyonlinelibrary.com]

and are combined collinearly through a dichroic mirror with the ps-beam in transmission and the fs-beam in reflection giving an interaction length of ~3 mm. After the intersection, all the beams are collimated, and the pump/Stokes and probe beams are filtered out by an angle-tuned band-pass filter (Semrock). The CARS and CCARS signals are separated in a polarization-sensitive two-detection channels coherent imaging spectrometer (400 mm, with ~3040 lines/mm), where the two orthogonally polarized signals are dispersed and collected in two distinct portions of the sCMOS camera sensor (Zyla, Andor).

A gaseous flow of nitrogen in binary mixture with argon (with concentrations in the range 30%–80%) is channelled through a 10-mm diameter pipe with unobstructed optical access. The mixture composition is varied by changing the flow rate of nitrogen (0.14–1.79 L/min), while maintaining a fixed flow rate of argon (0.34 L/min). The gases are properly mixed and provided to the measurement location at a steady-state ~1-m/s near-laminar flow conditions (Reynolds number ≈3000).

4 | EXPERIMENTAL RESULTS

In the present work, we examine the generation of the CARS and CCARS signals in the aforementioned mixtures at ambient conditions. CARS spectroscopy in homogeneous gas-mixtures, e.g. in optical cells and in one-dimensional/two-dimensional (1D/2D) flames, or in long-distance focusing applications, such as power plants and industrial furnaces, is often carried out with a collinear arrangement of the pump, Stokes and probe beams. In this beam geometry, the signal is maximized due to the fulfilment of the phase-matching condition and to the interaction length being solely limited by twice of the Rayleigh length of either one of the focused beams. The efficiency of the CCARS signal generation in the gas

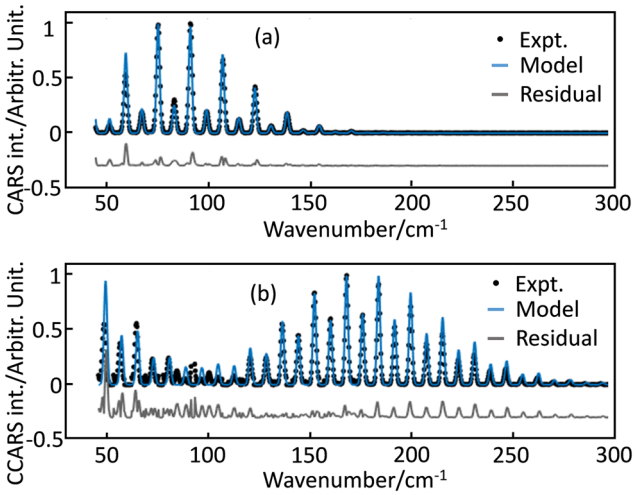

FIGURE 3 Coherent anti-Stokes Raman scattering (CARS) (a) and cascaded CARS (CCARS) (b) spectra from nitrogen at $T = 293$ K and best-fit model [Colour figure can be viewed at wileyonlinelibrary.com]

phase is ~1% for a given set of parameters, due to the relatively low number density of the scattering molecules, comparing with the condensed phase.[20] Although the conversion efficiency of the CARS field to the CCARS one is rather low, the cascaded signal can potentially interfere with the spectral signature of chemical species present in low concentrations. On the other hand, the CCARS signal may also be used for other quantitative measurements, as we outline in the following.

Figure 3 shows single-shot CARS and CCARS spectra recorded in a gaseous flow of pure nitrogen at a temperature of 293 K. The spectra are acquired with a pulse energy of 100 μJ for the degenerate pump/Stokes pulse and 2 μJ for the probe pulse, at a probe delay of ~35 ps. The signals are generated with orthogonal polarizations and detected simultaneously in two distinct channels on the same detector frame. The first channel contains the

S-branch CARS spectrum and is attenuated with a neutral density filter by two orders of magnitude to avoid camera saturation. The second channel contains a discrete spectrum, where each line corresponds to the overlapped S- and O-branch CCARS signals, scattered from the Raman coherence by the different CARS spectral lines, each one acting as an individual probe. The CCARS signal is computed, using the time-domain CARS model described above, for a given CARS signal. It should be noticed that in the CCARS spectrum the ratio of even and odd lines for N_2 is close to 4:3, while for the CARS signal it is known to be 4:1. Each line in the CCARS spectrum actually comprises multiple CCARS lines originated from different CARS lines. Each CARS spectral line serves as a probe producing the whole S- and O-branch rotational spectrum. The separation between even and odd N_2 adjacent spectral lines is ~4B, with B being the rotational constant of the Raman-active species (~2 cm^{-1} for N_2), and the first S-branch spectral line is ~6B shifted from the probe spectral line. As a result, the CCARS spectrum consists of multiple CARS spectra shifted by ~4B from each other. The spectral lines from the cascaded process, which are thus shifted ~2B apart from the CARS lines, can readily be isolated with high-resolution detection. When several types of rotational Raman-active molecules are present in the gas mixture (e.g., N_2 and O_2), the corresponding CCARS spectral lines might overlap and interfere with CARS lines. Therefore, polarization separation of CARS and CCARS can be even more important in gas mixtures. One may notice residual lines in the second channel, caused by imperfections in the polarization optical components in use, resulting in a slight contamination of this channel by the unattenuated CARS signal.

According to Equation 3, the CARS signal intensity scales as $I_{CARS} \propto I_1 I_2 I_3$. In a two-beam CARS experiment, where the pump and Stokes beams are degenerate, this entails a quadratic dependence of the CARS signal intensity on the energy of single degenerate pump/Stokes femtosecond pulse, containing both the pump and Stokes photons. In the case of the CCARS signal, the intensity scales as $I_{CCARS} \propto I_1^2 I_2^2 I_3$ and, therefore, it has quartic (i.e., 4th power) dependence on the pump/Stokes pulse energy. Figure 4a shows the measured CARS and CCARS signal intensities for various pump/Stokes pulse energies within the range 10–25 μJ: the observed signal scaling law is in agreement with Equations 3 and 5. However, a further increase of the pulse energy results in a change of the trend for both signals as displayed in Figure 4b. The CARS signal starts scaling linearly, and the CCARS signal scales quadratically in the range 30–120 μJ. An operation at higher pulse energy leads to higher precision of the number density measurement decreasing the relative

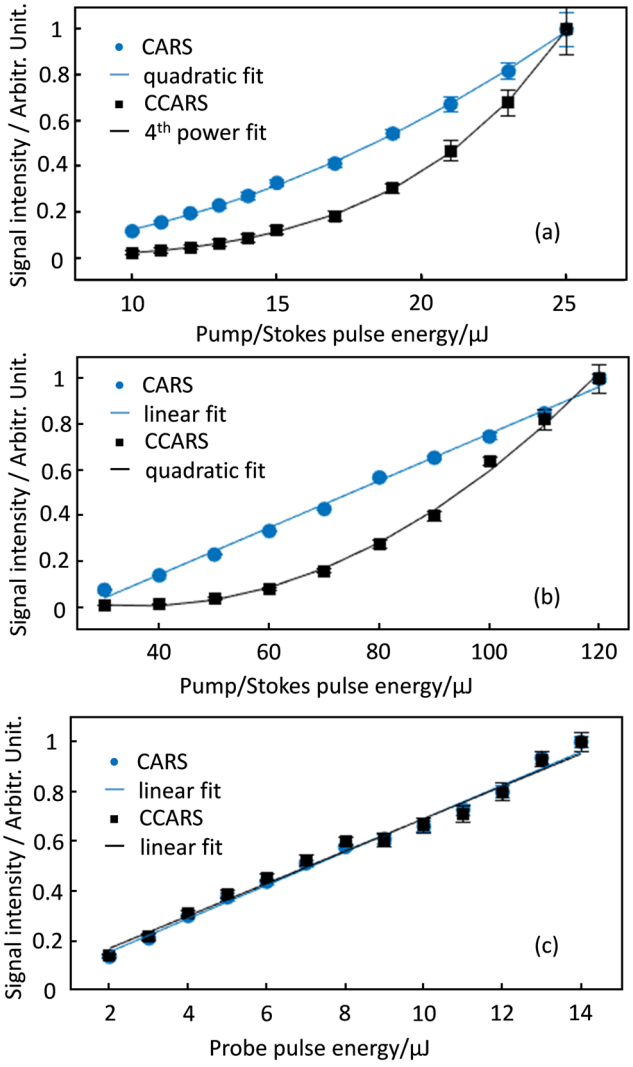

FIGURE 4 The coherent anti-Stokes Raman scattering (CARS) and cascaded CARS (CCARS) signal strengths as functions of the pump/Stokes pulse energy in the range (a) 10–25 μJ and (b) 30–120 μJ. The CARS signal strength is balanced to a factor of ~6 times the cascaded CARS signal strength, after attenuating the CARS signal by two orders of magnitude. (c) Linear dependence of both the CARS and CCARS signals on the probe pulse energy [Colour figure can be viewed at wileyonlinelibrary.com]

standard deviation from 4.5% to 1.5% for the CARS signal and 17.0% to 5.3% for the CCARS signal. At around 120-μJ pulse energy, a weak plasma channel can be observed by the naked eye: this is commonly referred to as a 'fs-laser-induced filament'.[30] In this study, filamentation is not a desirable phenomenon, as it results in potentially less stable excitation of the rotational Raman coherence and, consequently, reduced precision of the technique. A dedicated study is deemed necessary to investigate the deviation of the CARS signal scaling law from quadratic. Currently, we suppose that the linear signal scaling is accompanied by the initiation of the

filament in the probe volume via competing Kerr effect, self-phase modulation, and multiphoton ionization, eventually resulting in ionization of N_2 and the development of the filament.[31] Moreover, as it follows from Equations 3 and 5, and is demonstrated in Figure 4c, both signals scale linearly with the probe pulse energy. The standard deviation, calculated from the integrated signal intensity without normalization, is larger for the CCARS signal. This behaviour is not surprising as the CCARS has a higher order dependence on the pump/Stokes pulse energy, interaction length and scatterers number density. Moreover, as mentioned above, the CARS signal is attenuated with a neutral density filter, which explains even less pronounced deviations in comparison with the CCARS signal. The linear scaling of both signals with the probe pulse energy allows for correlated control of the signal levels, while preserving the ratio between them.

An inherent characteristic of CARS spectroscopy is the strong sensitivity of the signal to the number density of scatterers in the probe volume. When assuming the gas-phase medium to be described by the ideal gas law, the number of molecules in a given control volume can be determined as a function of pressure and temperature, according to $N = PV/(k_B T)$. Given the linear dependence of the nonlinear susceptibility of the medium on the density of scattering molecules (i.e., $\chi^{(3)} \sim N$), the well-known quadratic dependence of the CARS signal thus follows $I_{CARS} \sim N^2$. This quadratic dependence enters Equation 5, for the intensity of the CCARS signal, resulting in the following relation: $I_{CCARS} \sim N^4$. Therefore, the CCARS process is even more sensitive to variations in the number density of the Raman-active species in the probe volume. Figure 5a shows the CARS and CCARS signal strengths as measured from nitrogen at various concentrations (ranging from 30% to 80%) in the binary mixture with argon. Each data point consists of an integrated signal averaged over 100 single-shots, acquired over ~1 s. In agreement with what predicted by the theory, the CARS signal depends on the number density quadratically, whereas the CCARS signal depends on the number density to the power of four.

The polarization-divided detection employed in the present work allows us to record both signals simultaneously and to deduce the ratio of the CARS and CCARS signal intensities, in order to estimate the number density of the scattering species with high sensitivity as: $I_{CCARS}/I_{CARS} \sim N^2$. The temperature of the gas-mixture can be assessed from the CARS spectrum in the first channel. Subsequently, the number density of nitrogen in the mixture is estimated from the ratio of the integrated CARS signal and several of the most intense lines of the CCARS signal, as each line in the cascaded spectrum contains contributions from all the

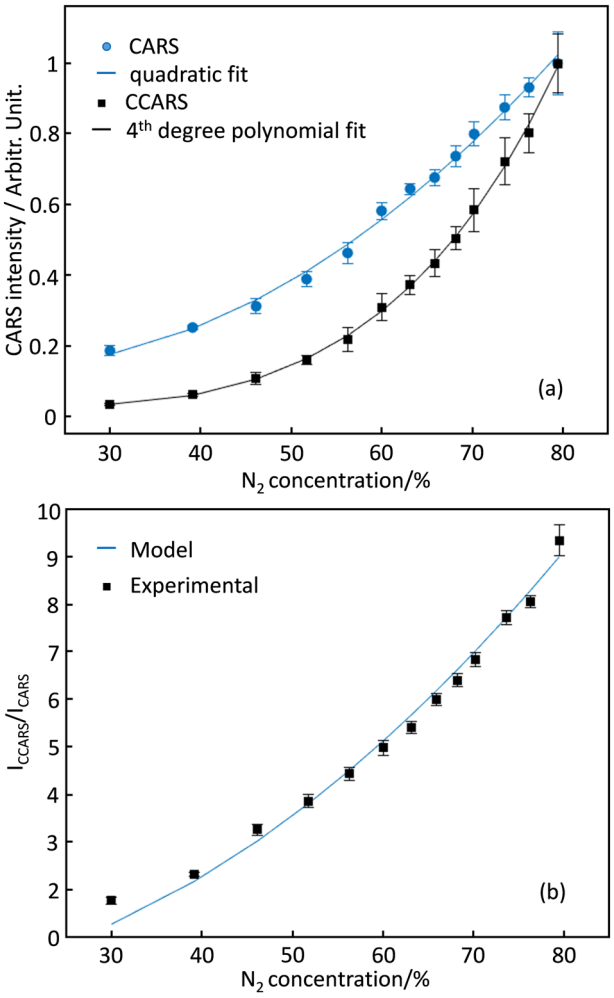

FIGURE 5 (a) Simultaneous coherent anti-Stokes Raman scattering (CARS) and cascaded CARS (CCARS) integrated signal strengths, recorded in nitrogen at various concentrations (in the range 30%–80%) in a binary mixture with argon. (b) The signal ratio of the CCARS and CARS signals at different nitrogen concentrations in the binary mixture. The functional dependence is compared to the ideal gas law [Colour figure can be viewed at wileyonlinelibrary.com]

CARS transitions serving as probe pulses. At first, a calibration of this signal ratio needs to be carried out for known values of the number density and temperature. In a practical scenario, this can be obtained in pure nitrogen at room temperature (i.e., $T = 293$ K). We acquire a series of CARS and CCARS spectra in a flow of premixed nitrogen and argon with known concentrations in the range 30%–80%. The intensity ratio of the experimental and theoretical CARS and CCARS signals is displayed in Figure 5b, for the different N_2–Ar concentrations. The second data point corresponding to a ~80% concentration of nitrogen is employed as the calibration point. A good agreement with the theoretical values is obtained across the entire range, with a

systematic deviation of <5%. This consistency is clearly satisfactory, and it allows us to speculate that the suggested technique can be employed for the measurement of absolute number density on a wide number density range. The use of the ratio between the CARS and CCARS signal intensities cancels the uncertainty of the probe pulse energy, and shot-to-shot variations in the pump/Stokes pulse energy are minute with current commercially available ultrafast regenerative amplifier systems. In this experiment, the pump/Stokes and probe pulses were operated with relatively low pulse energies, 70 and 5 μJ, respectively, such that the CARS signal was close to saturation of the camera at the maximum nitrogen concentration. Once calibrated at high number density and low probe pulse energy, sufficient to generate CCARS, the current technique can be used to measure a wide range of number densities of scattering molecules by increasing the available probe pulse energy without the need to recalibrate the spectrometer, as variations in the probe energy do not affect the ratio between the CARS and CCARS signals. In future work, in our laboratory, we will also investigate the performance of the current technique in more complex gas mixtures, as well as the use of combined CARS/CCARS to quantify pressure in situ with high-sensitivity.

5 | CONCLUSIONS

In conclusion, we have investigated the generation of a CCARS signal in nitrogen at ambient temperature and pressure. The probability of the cascaded coherent Raman scattering process is increased in a collinear arrangement, where the incident beams are focused jointly along the same beam propagation axis. In the present work, we employed two collinear beams, one delivering an ~35-fs pump/Stokes pulse at 800 nm, and the second one providing an ~15-ps probe pulse at 400 nm to the probe volume, for the generation of pure-rotational CARS photons. These photons underwent further inelastic scattering from the Raman coherence induced along the ~3-mm fs-beam focus, and resulting in a strong CCARS signal. The detected intensity of the CCARS signal was about two orders of magnitude weaker than the intensity of the CARS signal. On the one hand, the CCARS process can be seen as an unwanted phenomenon, which might complicate the analysis of the CARS spectrum. In this respect, it needs to be taken into account when analysing minor spectral signatures at relatively high number density of scattering molecules. Polarization control of the CARS signal generation was successfully implemented in order to produce the CARS and CCARS signals with orthogonal polarizations. In this arrangement, the CCARS signal can be effectively rejected. On the other hand, the CCARS signal has a fourth-order dependence on the number density of the scattering molecules in the mixture. This dependence is appealing for high-sensitivity diagnostics in the gas phase. In a set of measurements performed on varying concentration of nitrogen in binary mixture with argon, the significant variation in the ratio of the simultaneously detected CARS and CCARS signals was used to measure the absolute concentration of nitrogen. We demonstrated that the ratio of CARS and CCARS signals is independent of the probe pulse energy employed, which can be a promising approach to wide-range absolute concentration measurements in the gas phase.

ACKNOWLEDGEMENTS

We gratefully acknowledge the financial support provided by the Netherlands Organization for Scientific Research, obtained through a Vidi grant (15690) in the Applied and Engineering Sciences domain.

ORCID

Dmitrii Kliukin https://orcid.org/0000-0003-2582-3479
Francesco Mazza https://orcid.org/0000-0003-4406-8034
Alexis Bohlin https://orcid.org/0000-0003-4383-8332

REFERENCES

[1] A. C. Eckbreth, *Laser Diagnostics for Combustion Temperature and Species*, 2nd ed., Gordon and Breach, Amsterdam **1996**.
[2] D. R. Richardson, R. P. Lucht, W. D. Kulatilaka, S. Roy, J. R. Gord, *Appl. Phys. B Lasers Opt.* **2011**, *104*, 699.
[3] T. Lang, M. Motzkus, *J. Opt. Soc. Am. B* **2002**, *19*, 340.
[4] J. D. Miller, M. N. Slipchenko, T. R. Meyer, H. U. Stauffer, J. R. Gord, *Opt. Lett.* **2010**, *35*, 2430.
[5] L. Castellanos, F. Mazza, D. Klyukin, A. Bohlin, *Opt. Lett.* **2020**, *45*, 4662.
[6] J. Barros, M. Scherman, E. Lin, N. Fdida, R. Santagata, B. Attal-Tretout, A. Bresson, *Opt. Express* **2020**, *28*, 34656.
[7] T. L. Courtney, N. T. Mecker, B. D. Patterson, M. Linne, C. J. Kliewer, *Appl. Phys. Lett.* **2019**, *114*, 101107.
[8] S. P. Kearney, *Combust. Flame* **2015**, *162*, 1748.
[9] J. E. Retter, G. S. Elliott, S. P. Kearney, *Combust. Flame* **2018**, *191*, 527.
[10] D. Escofet-Martin, A. O. Ojo, J. Collins, N. T. Mecker, M. A. Linne, B. Peterson, *Opt. Lett.* **2020**, *45*, 4758.
[11] S. P. Kearney, D. R. Richardson, J. Retter, C. Dedic, P. M. Danehy, in AIAA Scitech 2020 Forum, **2020**, p. 770.
[12] B. D. Patterson, Y. Gao, T. Seeger, C. J. Kliewer, *Opt. Lett.* **2013**, *38*, 4566.
[13] A. Compaan, E. Wiener-Avnear, S. Chandra, *Phys. Rev. A* **1978**, *17*, 1083.
[14] D. A. Blank, L. J. Kaufman, G. R. Fleming, *J. Chem. Phys.* **1999**, *111*, 3105.
[15] F. Belli, A. Abdolvand, W. Chang, J. C. Travers, P. S. J. Russell, *Optica* **2015**, *2*, 292.

[16] K. Krupa, K. Baudin, A. Parriaux, G. Fanjoux, G. Millot, *Opt. Lett.* **2019**, *44*, 5318.
[17] P. A. Carpeggiani, G. Coccia, G. Fan, E. Kaksis, A. Pugžlys, A. Baltuška, R. Piccoli, Y. G. Jeong, A. Rovere, R. Morandotti, L. Razzari, B. E. Schmidt, A. A. Voronin, A. M. Zheltikov, *Optica* **2020**, *7*, 1349.
[18] Z. Liu, J. Yao, H. Zhang, B. Xu, J. Chen, F. Zhang, Z. Zhang, Y. Wan, W. Chu, Z. Wang, Y. Cheng, *Phys. Rev. A* **2020**, *101*, 043404.
[19] S. Roy, P. J. Wrzesinski, D. Pestov, M. Dantus, J. R. Gord, *J. Raman Spectrosc.* **2010**, *41*, 1194.
[20] V. B. Pelegati, B. B. C. Kyotoku, L. A. Padilha, C. L. Cesar, *Biomed. Opt. Express* **2018**, *9*, 2407.
[21] L. Gong, W. Zheng, Y. Ma, Z. Huang, *Nat. Photonics* **2020**, *13*, 115.
[22] J. D. Miller, S. Roy, M. N. Slipchenko, J. R. Gord, T. R. Meyer, *Opt. Express* **2011**, *19*, 15627.
[23] C. Yang, D. Escofet-Martin, D. Dunn-Rankin, Y. C. Chien, X. Yu, S. Mukamel, *J. Raman Spectrosc.* **2017**, *48*, 1881.
[24] R. W. Boyd, *Nonlinear Optics*, 2nd ed., Academic Press, Boston **2008**.
[25] A. Bohlin, B. D. Patterson, C. J. Kliewer, *J. Chem. Phys.* **2013**, *138*, 81102.
[26] A. Bohlin, C. J. Kliewer, *Appl. Phys. Lett.* **2014**, *104*, 31107.
[27] S. Akhmanov, A. Bunkin, S. Ivanov, N. Koroteev, *Sov. J. Exp. Theor. Phys.* **1978**, *47*, 667.
[28] F. Vestin, M. Afzelius, P. E. Bengtsson, *Proc. Combust. Inst.* **2007**, *31*, 833.
[29] F. Mazza, L. Castellanos, D. Kliukin, A. Bohlin, *Proc. Combust. Inst.* **2021**, *38*, 1895.
[30] J. H. Odhner, D. A. Romanov, R. J. Levis, *Phys. Rev. Lett.* **2009**, *103*, 075005.
[31] H. Xu, E. Lötstedt, A. Iwasaki, K. Yamanouchi, *Nat. Commun.* **2015**, *6*, 6.

How to cite this article: Kliukin D, Mazza F, Castellanos L, Bohlin A. Cascaded coherent anti-Stokes Raman scattering for high-sensitivity number density determination in the gas phase. *J Raman Spectrosc*. 2021;1–9. https://doi.org/10.1002/jrs.6120